STUDYING THE HETEROGENEITY OF DISCONTINUOUS FIBER COMPOSITES USING A NEW FULL-FIELD STRAIN MEASUREMENT SYSTEM

K. Johanson, L. T. Harper*, M. Johnson, A. Kennedy, N. A. Warrior
University of Nottingham
* Corresponding author (lee.harper@nottingham.ac.uk)

Keywords: *Composites, discontinuous fiber, strain measurement*

Abstract

In this paper a new multi camera digital image correlation (DIC) system is used to view strain fields from opposing surfaces of discontinuous carbon fiber composites loaded in tension. The system is investigated to understand if DIC can be used to correlate the cause of damage initiation to the underlying fiber architecture within heterogeneous composites. Results indicate that whilst potential final failure sites can be detected at low global strains in the form of strain concentrations, they are not always evident on both sides of the sample. Localized variations in the strain fields exist at the meso (tow) scale in materials with stochastic architectures. Studying the development of strains on both sides of the sample at even modest global strains gives an early indication of where damage is likely to initiate, which can then be related back to underlying architectural features identified by ultrasonic C scan. However, pin-pointing the specific region of ultimate failure is not possible using these techniques alone. This phenomenon is dependent on the specimen thickness and the fiber volume fraction, which explains why ordinarily it can be difficult to associate the location of fracture sites with features observed in conventional single-sided DIC strain profiles.

1 Introduction

Composites can be made cost effectively and in sufficient volumes using the Directed Carbon Fiber Preform (DCFP) process, as potential replacements for steel and aluminum components for niche vehicles [1]. However, as with most discontinuous fiber architectures DCFP is heterogeneous, which results in high material variability and complicates the prediction of mechanical properties compared with textiles. Modified rule of mixtures techniques and classical laminate theory provide sufficiently accurate global stiffness predictions [2-6] for discontinuous fiber architectures, but these 'smeared' approaches fail to account for the complex failure mechanisms which influence the onset and propagation of damage. Various finite element models have been developed in attempts to predict failure, establishing how the micro mechanical behavior contributes to failures at the meso and macro scale [7-9]. Traditional methods of measuring global strains, such as strain gauges or extensometers are limited for validating these models, and therefore full field strain analysis techniques are utilized as a comparator [10].

Moiré interferometry has been demonstrated as a useful tool for visualizing full strain fields and the local gradients in specimens under tension [11, 12]. This technique has been successfully implemented to visualize through specimen strain fields in laminated composites [13], giving confidence that localized gradients can be identified using this technique. However, existing systems require highly coherent light, which is only possible with expensive and cumbersome long cavity lasers. The other major limiting factor is its sensitivity to vibration, which restricts its application to laboratory conditions.

Through the development of a 2 dimensional technique, which was later extended to 3 dimensions; digital image correlation (DIC) has been developed [14-17] as a practical and widely accepted method of full field strain measurement [18]. The displacements, and therefore induced strains, can be calculated for a specimen by comparing a succession of images taken over time during mechanical loading. This technique is much less susceptible to vibration than interferometry,

partially due to the lower spatial resolutions involved, and the 3D method has the added benefit of utilizing two images; eliminating image-plane displacement gradients and the errors they introduce in strains commonly experienced with the 2D approach [19].

Whilst the use of this technique is well established, strain fields are typically determined from just one side of the specimen. This is satisfactory for characterizing the behavior of homogeneous, isotropic materials, but it is logical that discrepancies may exist between the strain fields from the two outer surfaces for composites with random fiber architectures. Feraboli et al [20, 21] reported that localized defects, generally associated with voids or resin rich areas, are not necessarily indications of sites for ultimate failure in these materials, suggesting more complicated mechanisms may determine where failure or damage is initiated. However, it is possible that critical features in the strain fields were being overlooked, since strain data was only collected from one side of each sample.

It is therefore rational to use a multi-camera DIC system to observe the strain fields on both sides of the specimen in stereo. Previous attempts to examine strain fields on opposing sides of paperboard samples [22] were problematic, with only a single camera used to view each side of the specimen. One side was also observed in a reflecting mirror, which was one potential source of error associated with the translation, rotation and scaling used to map the analysis images.

Where multiple DIC camera systems have been used in the literature [23, 24] it was not to view opposing faces. Up to 4 cameras were used by Laurin et al [23] to determine the properties of unidirectional laminates. Two cameras were placed either side of specimens to view the thickness of the laminate during a four point bend test, clearly demonstrating the ability to use DIC to identify through-specimen differences in the strain fields of multi-layer laminates. Further experimentation demonstrated the ability to identify both local and global buckling of an impacted specimen under compression. Tensile testing was also carried out but with only a single camera observing the specimen. Any out of plane movement (Z Plane) was registered as a movement in the X and Y directions, leading to further inaccuracies in the reported strains.

The aim of this paper is to implement a multi-camera DIC approach to collect full-field strains from opposing surfaces of discontinuous carbon fiber composite samples. These will be compared with ultrasonic C-scans to investigate if the surface strain distribution directly correlates with areas of attenuation, caused by local variations in the fiber areal mass through the thickness of the structure. Ultrasonic C-scanning has previously been considered as a non-destructive method for evaluating the fiber distribution within discontinuous architectures [21], but it was concluded that it was of little value due to difficulties in interpreting results and differentiating between poor attenuation and “defects”. Greater success was reported for laminated composites however, where delamination affected larger areas [25].

2 Methodologies

2.1 Manufacture of composite plaques

Three materials were chosen for the experimental work; mild steel, a non-crimp fabric (NCF) composite and a discontinuous fiber architecture. Steel was selected for system calibration, due to its homogeneous isotropic properties. NCF was chosen as an orthotropic benchmark material for comparison against the quasi-isotropic discontinuous material.

2.1.1 Preforms

For the NCF samples, 400 mm x 300 mm preforms were created by hand laminating individual plies of 200gsm/PW-BUD/T700SC 12K 50C/0600mm UD CF NCF (supplied by Sigmatex) into a tool. 12 plies were placed at alternating 0° and 90° orientations for a 3mm thick sample, giving a volume fraction in the region of 40% for the finished plaque. A second unbalanced architecture was created with alternating plies, but plies 8 and 9 were placed in the same orientation to achieve a preform where both external plies were in the 0° orientation. 3%wt Reichhold Pretex 110 binder was added between plies and the preform was compacted and cured at 120°C for 5 minutes to stabilize.

DCFP preforms were created using an automatic process [26]. A revolving chopper head randomly deposited orientated carbon tows, cut to 15mm

lengths from a continuous spool of Toray T700 60E 12k. The head moved across an expanded metal grid, through which a vacuum was drawn, depositing fibers in a 600 mm x 400mm region. Fiber was initially deposited following a series of North-South linear paths across the entire area, and then completed by depositing in an East–West direction. Binder was applied along with the fibers and the process was repeated until the desired volume fraction was met. All preforms were consolidated in a press before being punch cut to fit the 400mm x 300mm Resin Transfer Mold (RTM) tool.

2.1.2 Resin Transfer Molding

Both NCF and DCFP preforms were injected with Huntsman XU3508 resin in a vacuum assisted closed mold tool. The resin was preheated to 80°C and the tool temperature maintained at 90°C during the 15 minute injection cycle, at pressures of up to 5 Bar. Plaques were then cured for 4 hours at 110°C before being removed from the press and air cooled for 2 hours. Five plaques were created in total, with details presented in Table 1.

2.2 Preparation of Specimens and DIC System Calibration

Dog bone samples (dimensions as shown Figure 1) were milled from the completed composite plaques. High strength rolled steel samples were also milled from a flat strip 50 x 3mm. To ensure a suitable specimen size the dog bones were created at 38mm wide [27] and individual specimens were prepared with a stochastic speckle pattern on the front and rear faces, using water based model maker's paint. A white base layer was initially sprayed, onto which a black speckle pattern was applied using aerosol paint. Significant effort was made at this stage to optimize the size and distribution of the pattern to ensure image data was being collected across the whole of the region of interest (ROI) for the entire duration of the test. Too fine or too large a pattern resulted in data being lost across the sample. Each specimen had a horizontal line drawn, perpendicular to the sample edge, across the width of each surface. This was used during the post processing phase to align the coordinate system for the software graphics with that of the actual specimen and was designated the X-axis, with the direction of tensile elongation defined as the Y-axis and the Z- axis the through thickness of the specimen.

Full field strain results were measured using a Dantec Dynamics Digital Image Correlation System (Figure 2). The system consisted of 4 off 5 Megapixel CCD cameras with 28mm lenses. In a conventional 2 camera Digital Image Correlation (DIC) system, one camera is typically used as a reference. Within the image of this camera the points which are to be evaluated are defined on a grid basis and discretized into facet subsets. These facets can then be identified within subsequent images, from the same or a second camera, and their new position identified relative to the reference. A limitation to this approach is that it is only possible to measure the displacement on surfaces which are within the view of the reference camera, this leads to restrictions in its use, particularly on curved objects. To improve this situation a third camera can be added to the set-up.

Dantec Dynamics have developed a cluster based approach for the multi camera analysis. The points to be evaluated in this method are not defined by a reference camera image, but by a virtual object, created from the convergence of the images from the various cameras involved. The elimination of the reference image allows cameras to be positioned to view different areas of the test specimen, with the limitation that at least 2 cameras need to have visibility of any region for analysis. The cameras also need to be rigidly mounted to prevent relative movement with each other. With a suitable mount and 8 cameras this system can be used on cylindrical specimens, giving a full 360° view, without the need to stitch the data. A specially created double sided calibration target is required for viewing two opposing sides of the specimen when using four cameras. Each side of the target has its own unique coordinate system for correlation. By knowing the relative positions of these two coordinate systems a single coordinate system can be defined and used for the analysis of the specimen.

2.3 Tensile Testing

Specimens were tested on an Instron 5581 Universal testing machine. Tensile samples were elongated at a rate of 1mm/min and strain data collected using the described equipment with a sampling rate of 1Hz in accordance with BS2782; Method 326F: 1997.

Average specimen width and thickness were calculated from 5 measurements taken across the ROI for each part. Tensile modulus was evaluated over the range of 1000 to 3000 micro strain for all samples.

The steel sample was used to provide confidence in the system set up and to provide a benchmark for the other materials. As a homogenous ductile material with well published results for mechanical properties and failure modes, the strain fields were expected to be uniform through the part thickness.

Strains are calculated from the deformation gradient tensor $\mathbf{F} = \nabla \boldsymbol{x}$ which can be decomposed into a rotation and stretch tensor

$$\boldsymbol{F} = \boldsymbol{RU} \quad (1)$$

The rotation element is eliminated leaving the Cauchy-Green deformation tensor

$$\boldsymbol{C} = \boldsymbol{F}^T\boldsymbol{F} = \boldsymbol{U}^2 \quad (2)$$

This can be used to calculate the Green - Lagrangian strains

$$\boldsymbol{E} = \frac{1}{2}(\boldsymbol{C} - \boldsymbol{I}) \quad (3)$$

The average lagrangian strains in the Y direction from the DIC analysis were plotted against stress, calculated from the force channel of the Instron equipment, to determine tensile modulus (Figure 3). A separate modulus value was calculated for each surface of the sample. Strains were extracted over rectangular polygons created across the surface regions. Within the current beta version of the software, the corners of the polygons do not print through to both sides of the specimen, but individual points can be created which do appear on both surfaces. Therefore 4 points are first defined as the control corners over which the polygon corners are manipulated to be coincident. With the possibility of errors being included, due to the manual process of alignment, a study using a steel specimen was conducted to determine the sensitivity of the results to this process. A polygon was drawn on a single side of the sample, then deleted and redrawn over the defined corner points on 5 separate occasions. It was found that the modulus values calculated from the extracted polygons varied by less than 0.027%. Therefore, it was concluded that no significant error would be introduced through this manual process, provided care was taken in the alignment of the points.

A second study was conducted to evaluate the size and location over which the polygon is drawn to establish any effects that this may have on the strain results. Two polygons were evaluated against each other. The largest polygon was approximately 100mm in length and covered the entire width, named Gauge 1. Gauge 2 was created at approximately 50mm in length, similar in dimensions to a mechanical extensometer (Figure 1). During the discretization stage the software breaks the surfaces into smaller regions called facets. For this work a facet size of 17 pixels square was used at the suggestion of Dantec, based on the high quality of images available from this set-up. The facets overlap each other and the level of overlap can be modified. Increasing the overlap results in a smoother strain map, but is detrimental to the computation times. Three different levels of overlap were included in this study to understand the significance on the calculated modulus (Table 2).

2.4 Comparison of DIC strains with Ultrasonic C-scans

With DIC strain fields available for both surfaces of a specimen, a comparison can be made by combining the two strain fields to give a pseudo through specimen image, which can be directly compared with an ultrasonic C scan. This effectively assumes that the strain gradient between the two surfaces is linear, which may be a poor assumption, but it conveniently provides a way of comparing both strain fields with a single C-scan to establish if there is a link between the local areal mass variation and the failure site of the specimen.

The DIC plots for strain in the Y direction were extracted from the Dantec software and converted to a weighted grey scale, using ImageJ® analysis software. The images were split into the three constituent color channels (red, blue and green); with areas of high strain clearly visible in both the red and blue channels without further manipulation. The blue channel was chosen for further processing and the image for surface 2 was mirrored horizontally and merged with the image of surface 1, applying a 50% opacity value to each. This

effectively calculates an average greyscale value for the combined images.
The failed 3mm DCFP samples were scanned using a pulse-echo technique and a 5MHz sensor. The C scan image was manipulated in InspectionWare64® software, firstly converted to a grey scale image (0-255) and then a minimum threshold of 110 applied, to highlight the areas where the signal had been attenuated.

3. Results and Discussion

3.1 Steel specimen benchmark analysis

The symmetrical strain distributions on the two sides of the steel sample are shown in Figure 5. The image was taken just prior to final failure at an applied strain of 15000μstrain. The central region has undergone significant plastic deformation and the location of final failure by shear is indicated by the white lines drawn at 45°.
A main effects diagram can be seen in Figure 4 for the study investigating the effect of gauge size (large, small), facet overlap (5, 9 and 12 pixels) and specimen side (Surface 1, Surface 2) on the tensile modulus for the steel sample. The average elastic modulus was calculated to be 192.3GPa, with a 1.19% coefficient of variation, using the different polygon gauges described above. Tensile modulus values calculated using the larger sized gauges were 1.2% higher than those from the smaller gauge. Modulus values calculated from Surface 1 were 0.75% higher than those calculated from Surface 2. The effects of change in facet overlap were similar on each side and significantly less important than gauge size and specimen side, showing no discernible trend. A general linear model analysis of variance (GLM Anova) was conducted in Minitab v16, but no statistical relevance was found for interactions within the results. In general, the errors calculated for all three variables studied were considered to be insignificant, confirming that the system was suitably calibrated and appropriate for assessing strain variations within the composite samples.
The larger gauge was chosen over the smaller gauge for all subsequent analyses of the composite samples, due to an insignificant increase in computation time. Facet overlap was also minimized to 5 pixels, since it had no distinguishable effect on results for the current application. Using these criteria, the difference in tensile modulus between the 2 surfaces for the steel sample was 0.24%.
Matching linear gauges were drawn on opposing surfaces of the steel specimen to investigate the difference in local strains across the two sides of the sample (Figure 1). Two gauge lengths were initially created for the steel specimen (120mm and 50mm), covering either the full specimen length or simulating the length of a centrally positioned contact extensometer. Global modulus values were calculated (Table 2) and they are within the range calculated from the polygon gauges (190.5GPa – 194GPa). The local strains along the 120mm long gauge are plotted in Figure 9 for both sides of the specimen. Strains are displayed as a Strain Concentration Factor (SCF) which is calculated as the local strain divided by the global average in the specimen, which provides a normalized scale for comparing against the composite samples. There is a smooth transition of strain along the gauge length to the point where the sample has deformed plastically. There is also good conformity in the results between each of the surfaces, as expected for a homogenous material.

3.2 Global stiffness variability of composite specimens

Table 3 shows the average tensile modulus values for the composite samples calculated from the large polygon gauges. Unlike the steel analysis where a single sample has been used, results are presented for 6 different DCFP composite samples and two NCF samples (2 repeats for each fiber architecture), each with a unique stochastic pattern on either surface.
There is only a small error (0.6% maximum) between the modulus values calculated from each side of the NCF samples, which is of the same order of magnitude as the steel. The error is higher for the DCFP samples (1.8% maximum) because of larger intra-plaque strain variations. This can be observed by comparing the full-field Lagrangian strain plots for each composite specimen in Figure 6 - Figure 8. Each figure shows the strain distribution on both sides of the specimen, with white lines indicating where final fracture(s) occurred. The images were taken immediately prior to failure (see Table 1 for

failure strains) and have been plotted using a maximum micro-strain scale of 50k for comparison against the steel sample.
The NCF samples exhibit consistent strain fields on both sides of the specimen at the macro level, with no early indication of where the specimen may fail. Images of the 3mm and 6mm 40% VF DCFP samples not only show significant variation in the strain field within each surface, consistent with variation at the fiber bundle level, but also variation in high strain areas which appear on one surface and not the other. This suggests that there are significant local strain gradients through the thickness of the sample as a result of the fiber architecture. Consequently for the 3mm thick DCFP specimen in Figure 7 for example, it is impossible to predict where the sample may fail as the applied strain develops, as there are strain concentrations of similar size and magnitude throughout the surface of the specimen. Final failure eventually occurs at the root of the radius at the top of the image, which may have been as a result of the machining process rather than the fiber architecture. However, there is only evidence of a high strain in that region on one side of the specimen, which would have been completely overlooked in a conventional DIC setup.
There are fewer prominent strain concentrations in the 2mm DCFP samples, but it is difficult to conclude if this is because of thickness effects or because the fiber volume fraction is lower (20%) and consequently the strain response is dominated more by the matrix material rather than the fibers.

3.3 Local strain variability in composite samples

The 120mm linear strain gauges have been used to quantify the strain variability between the two sides of each specimen, presented as normalized values of local strain divided by global average (strain concentration factors) for each specimen surface presented in Figure 6 - Figure 8.
Figure 10 summarizes the linear gauge data for the two NCF samples. Strains are uniform along the entire length of the gauges in all instances, with a variation within the ±20% range used in the literature for filtering the effects of noise [21]. The small variation that is evident within the strain patterns appear to have a regular saw tooth form, which resembles the spacing of individual fibers in the fabric. The patterns are unexpectedly consistent on plaques with 0°/0° and 0°/90° architectures on the outer surfaces. On closer inspection under a different X axis scale (figure not included) it can be seen that the pattern is more irregular than is apparent in these images. However, in Figure 6 there are clearly horizontal lines of strain variation, which are more prominent on surface 2. The DIC may be detecting some influence from the inter-tow resin rich regions in the ply immediately below the surface.
There are no regions indicating abnormally high strain or that failure could be expected in a particular local area of the NCF sample, even at such a late stage in the test (see Figure 6 and Figure 10). Failure was fiber dominated and occurred suddenly at two locations where the radii of the dog bone meet the gauge section, due to the notch sensitive nature of the material [28]. The average error between strain profiles from the two corresponding surfaces from each specimen was less than 20% in each case.
The variation seen in the DCFP linear gauges (Figure 11 and Figure 12) differs from that of the steel (Figure 9) and NCF (Figure 10), both along the gauge and between the two surfaces. The peaks and troughs are irregular in interval and height along the gauge length. For the 3mm sample for example, there are areas where the magnitude of the local strains from the two surfaces are well matched (at a distance of 8-22mm), but most areas appear unrelated (for example at 58-65mm and 105-110mm). The average error between the strain profiles for Surface 1 and Surface 2 of the 2mm, 3mm and 6mm DCFP samples are 240%, 199% and 91% respectively. The error clearly reduces as the homogeneity of the sample improves with increasing thickness.
Extreme peaks in the strain distribution are evident at a distance of 6, 70 and 112mm for the 3mm DCFP sample (Figure 11). High strains are only recorded on one side of the sample at these points, further demonstrating that local variation in strain can occur across the surface and through the thickness of the specimen. The local strain is 13.5 times higher than the global average at a Y distance of 70mm, which is the peak value for this particular specimen. However, this point is unrelated to the final failure point, as fracture occurs due to the high strain observed at a distance of 6mm (SCF=10). These high strain events are localized, with adjacent areas having strain magnitudes in line with the average for

the sample, highlighting the general heterogeneous nature of the DCFP material.
There is also a single area of high strain on Surface 1 of the 6mm DCFP specimen (graph not shown) and whilst this is the site of final failure, there is no evidence of a corresponding strain concentration on the rear surface. The local strain at this point (173k με) is the highest value recorded within any composite specimen, which is likely to be due to a local fracture or dislocation. The magnitude of these local strain concentrations appear to increase with sample thickness, but this can be attributed to the different global strains applied in each case. The strain images were captured just prior to final failure rather than at a consistent strain value, so the thicker samples were subjected to a higher strain (see Table 1).
In general, observations for the discontinuous materials are similar to those of Considine and Vahey [22], with extreme levels of strain being identified close to the point of failure. Individual points of high strain, the surface they fall on and their ability to be identified as points of interest are evident at lower levels of applied strain, as shown in Figure 13. However, there are substantially more points with higher than average local strain values, even if viewed with an applied "filtering" method, making it difficult to isolate where the failure will occur. Viewing full field strains on both sides of discontinuous materials ensures that the strain development in the region of ultimate failure is successfully captured, but identifying which of the various high strain regions will trigger final failure is not clear from this method alone.

3.4 The influence of local areal mass variability

One of the 3mm DCFP samples was ultrasonically inspected for comparison against the DIC strain profiles. Several regions can be identified in Figure 14 which correlate in location, shape and size between the strain image from the DIC and C-scan. Arguably the region of failure (A) in the DIC image shows the characteristic joining of strain concentrations, as discussed by Feraboli et al [20], but the center of the sample (C) shows similar patterning and it is difficult to conclude how a decision could be made as to which region would fail first at the current applied strain. Area B shows a distinctive 2 line pattern which can be picked out from both the DIC image and the C-scan. There are also obvious edge correlations at D and at the dark region on the left hand side of the sample, just outside area C. The different greyscale values for the two patterns in area B indicates that they are of different intensity. They both originate from the image of Surface 1 and may give an indication of depth of the feature within the sample. However, ultrasonic B scanning which should be able to identify attenuation in cross sections of the sample, proved inconclusive in attempts to correlate these features. Other non-destructive techniques such as Computed Tomography (CT scanning) may be more successful at correlating specific architectural features with strain signatures.

4 Conclusions

A new multi camera DIC cluster has been used to simultaneously collect full field strain data from two opposing surfaces of tensile specimens. Benchmark cases using steel and non-crimp fabric confirm that there is a good correlation between the tensile modulus values calculated from the front and rear surfaces (<2%). The multi-camera DIC approach is particularly valuable for measuring strain fields in heterogeneous materials, where surface strains differ due to fiber architectural features and defects.
The strain fields for the discontinuous fiber composites show variation within each surface, consistent with fiber bundle variation, but also differences can be observed between opposing surfaces of the same specimen. Some large strain concentrations which are responsible for final failure are only identifiable on a single surface and therefore would have been overlooked by a conventional single sided DIC set-up. There appears to be an increasing trend between the magnitude of the maximum local strain concentration within a sample and the specimen. Additionally, the strain distribution appears to be less varied for thicker samples.
Whilst the new DIC technique offers additional insight into the development of strain fields, highly strained regions on the outer surfaces are not necessarily an indicator of the area of ultimate failure, particularly as specimen thickness increases. Ultrasonic C-scanning has been used to study the local areal mass variation and there is a strong correlation between these results and strain

concentrations observed from the DIC strain analysis. However, there is insufficient information at this stage to conclude whether variations in the local areal mass dominate failure. Complementary techniques such as micro CT imaging are required to visualize underlying architectural features such as voids, bundle ends, fiber cross-overs etc. to enable the key failure mechanisms to be clearly identified.

Acknowledgements

The authors gratefully acknowledge the support of Dantec Dynamics for the development of the multi camera cluster and their technical support throughout this work.

References

[1] TURNER, T.A., et al., Low cost carbon-fibre based automotive body panel systems - a performance and manufacturing cost comparison. Journal of Automobile Engineering - Proceedings of the Institution of Mechanical Engineers Part D, 2008. 222(1): p. 53-64.

[2] HART-SMITH, L.J., The Ten-Percent Rule for preliminary sizing of fibrous composite structures, in 51st Annual Conference1992, Aerospace Materials. p. 10-16.

[3] HALPIN, J.C., Stiffness and expansion estimates for oriented short fiber composites. Journal of Composite Materials, 1969. 3: p. 732-734.

[4] BLUMENTRIT, B.F., B.T. VU, and S.L. COOPER, Mechanical properties of discontinuous fiber reinforced thermoplastics. II. Random-in-plane fibre orientation. Polymer Engineering and Science, 1975. 15(6): p. 428-436.

[5] CHRISTENSEN, R.M. and F.M. WAALS, Effective stiffness of randomly oriented fibre composites. Journal of Composite Materials, 1972. 6: p. 518-532.

[6] MANERA, M., Elastic properties of randomly oriented short fiber-glass composites. Journal of Composite Materials, 1977. 11: p. 235-247.

[7] PAN, Y., L. IORGA, and A.A. PELEGRI, Analysis of 3D random chopped fiber reinforced composites using FEM and random sequential adsorption. Computational Materials Science, 2008. 43(3): p. 450-461.

[8] HARPER, L.T., et al., Representative volume elements for discontinuous carbon fibre composites – Part 1: Boundary conditions. Composites Science and Technology, 2012. 72(2): p. 225-234.

[9] HARPER, L.T., et al., Representative volume elements for discontinuous carbon fibre composites – Part 2: Determining the critical size. Composites Science and Technology, 2012. 72(2): p. 204-210.

[10] GREDIAC, M., The use of full-field measurement methods in composite material characterization: interest and limitations. Composites: Part A, 2004. 35: p. 751-761.

[11] POST, D., R.CZARNEK, J.WOOD, D.JOH and S.LUBOWINSKI, Deformations and strains in adhesive joints by Moire interferometry, 1984, Virginia Polytechnic Institute and State University: NASA Langley.

[12] CORDERO, R.R., M.FRANCOIS, I.LIRA, C. VIAL-EDWARDS, Whole-field analysis of uniaxial tensile tests by Moire interferometry. Optics and Lasers in Engineering, 2005. 43(9): p. 919-936.

[13] JACKSON, W., P.G.IFJU, Through-the-thickness tensile strength of textile composites, 1994, NASA: Langley.

[14] CHU, T.C., W.F.RANSON, M.A.SUTTON and W.H.PETERS, Applications of Digital-Image-Correlation techniques to experimental mechanics. Experimental Mechanics, 1985. 25(3): p. 232-244.

[15] HELM, J.D., M.A.SUTTON, and S.R.MCNEILL. Three Dimensional Image Correlation for surface displacement measurement. in SPIE Videometrics III. 1994.

[16] HELM, J.D., S.R.McNEILL and M.A.SUTTON, Improved Three dimensional image correlation for surface displacement measurement. Optical Engineering, 1996. 35(7): p. 1911-1920.

[17] SUTTON, M.A., W.J.WOLTERS, W.H.PETERS, W.F.RANSON and S.R.McNEILL, Determination of displacements using an improved Digital Image Correlation method. Image and Vision Computing, 1983. 1(3): p. 133-139.

[18] BING, P., K.QIAN, H.XIE and A.ASUNDI, Two-dimensional digital image correlation for in-plane displacement and strain measurement: a review. Measurement Sceince and Technology, 2009. 20(062001): p. 17.

[19] LAVA.P, et al., Impact of lens distortions on strain measurements obtained with 2D digital image correlation. Optics and Lasers in Engineering, 2013. 51(5): p. 576-584.

[20] FERABOLI, P., et al., Defect and damage analysis of advanced discontinuous carbon/epoxy composite materials. Composites: Part A. Applied Science and Manufacturing, 2010. 41(6): p. 774-786.

[21] FERABOLI, P., et al., Stochastic laminate anology for simulating the variability in modulus of discontinuous composite materials. Composites: Part A, 2010. 41: p. 557-570.

[22] CONSIDINE, J.M., D.W.VAHEY. Full-field local displacement analysis of two-sided paperboard. in 61st Appita Annual Conference and Exhibition. 2007. Gold Coast.
[23] LAURIN, F., J.-S CHARRIER, D.LEVEQUE, J.-F MAIRE, A.MAVEL, P.NUNEZ, Determination of the properties of composite materials thanks to digital image correlation measurements. Procedia IUTAM, 2012. 4: p. 106-115.
[24] De ALMEIDA, O., F. LAGATTU, and J. BRILLAUD, Analysis by a 3D DIC technique of volumetric deformation gradients: Application to polypropylene/EPR/talc composites. Composites Part A: Applied Science and Manufacturing, 2008. 39(8): p. 1210-1217.
[25] AGGELIS, D.G., et al., Acoustic structural health montoring of copmposite materials : Dmage identification and evaluation in cross ply laminates using acoustic emission and ultrasonics. Composites Science and Technology, 2012. 72(10): p. 1127-1133.
[26] HARPER, L.T., et al., Characterisation of random carbon fibre composites from a directed fibre preforming process: Analysis of microstructural parameters. Composites Part A: Applied Science and Manufacturing, 2006. 37(11): p. 2136-2147.
[27] QIAN, C., L.T.HARPER, T.A.TURNER and N.A.WARRIOR, Notched behaviour of discontinuous carbon fibre composites; Comparison with quasi-isotropic non-crimp fabric. Composites Part A: Applied Science and Manufacturing, 2011. 42(3): p. 239-302.
[28] EDGREN, F., C. SOUTIS, and E.A. LEIF, Damage Tolerance analysis of NCF composite sandwich panels. Composite Science and Technology, 2008. 68(13): p. 2635-2645.

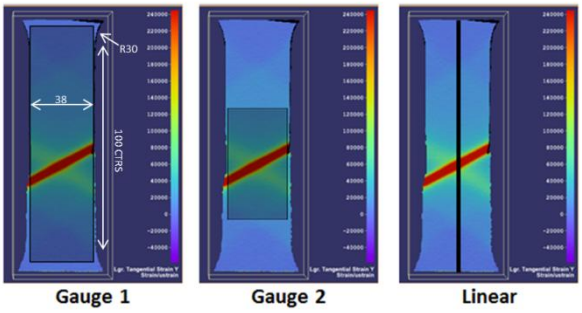

Figure 1: Size and position of polygons used to define gauges

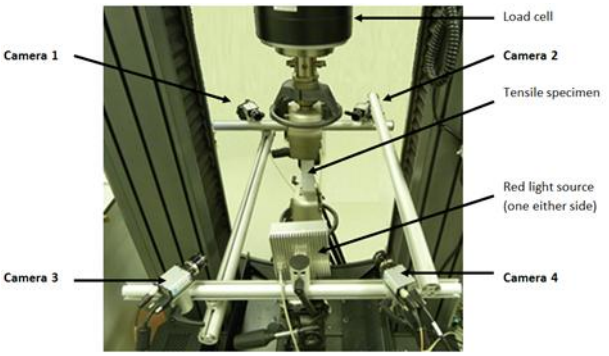

Figure 2: Multi camera DIC system

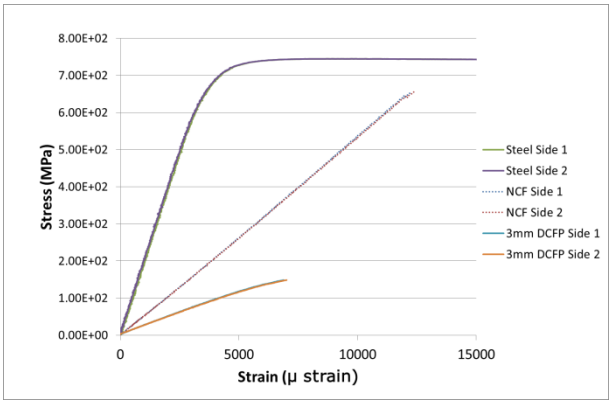

Figure 3: Stress versus strain curves for tensile modulus

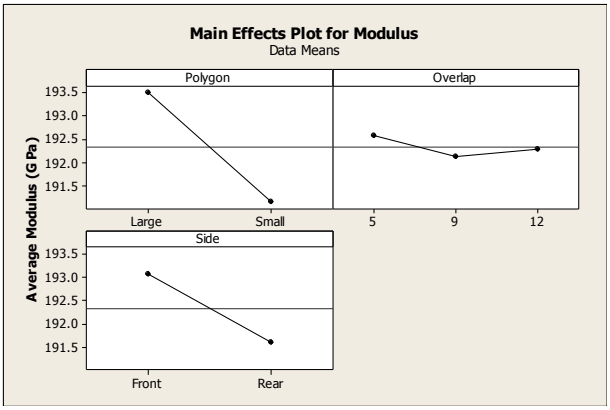

Figure 4: Main Effects Plot for the influence of polygon size (large, small), facet overlap (5, 9, and 12) and specimen side (Front, Rear) on the average tensile modulus (GPa)

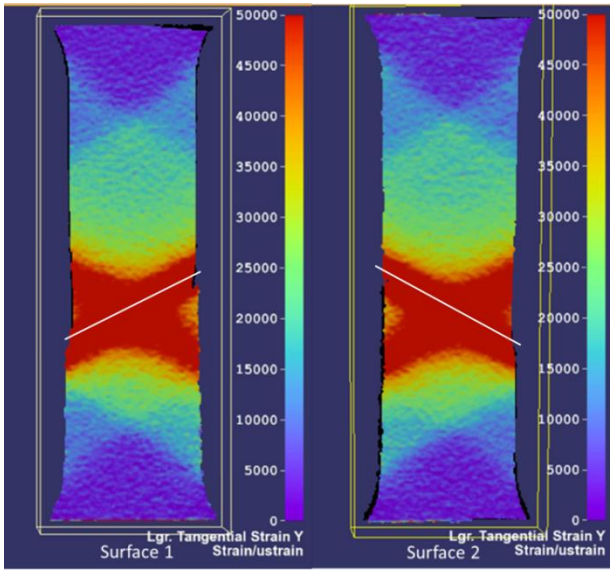

Figure 5: Full Field Strain Plot for 3mm Steel. Approximate plane of failure indicated by line

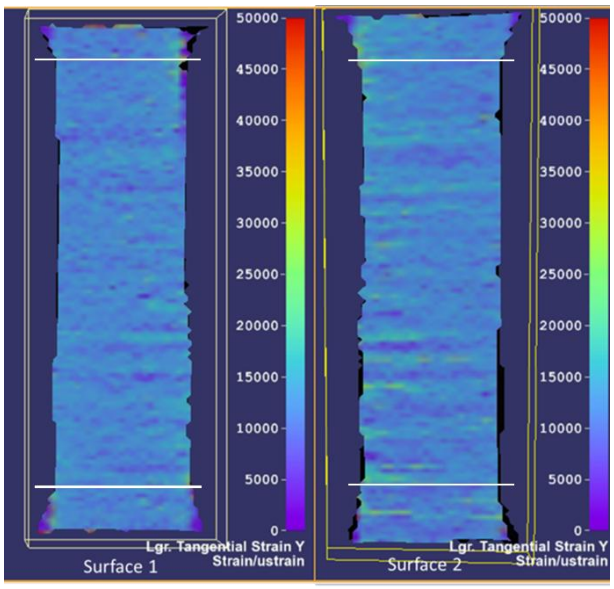

Figure 6: Full Field Strain Plot. 0°/90° NCF. Approximate plane of failure indicated by line

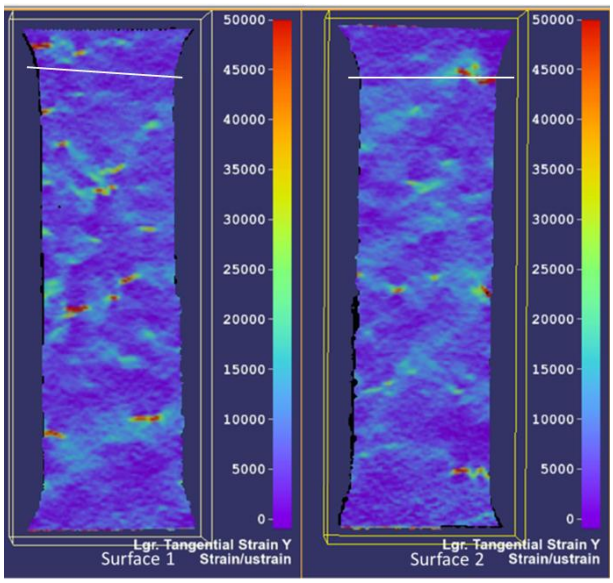

Figure 7: Full Field Strain Plot for 3mm DCFP. Approximate plane of failure indicated by line.

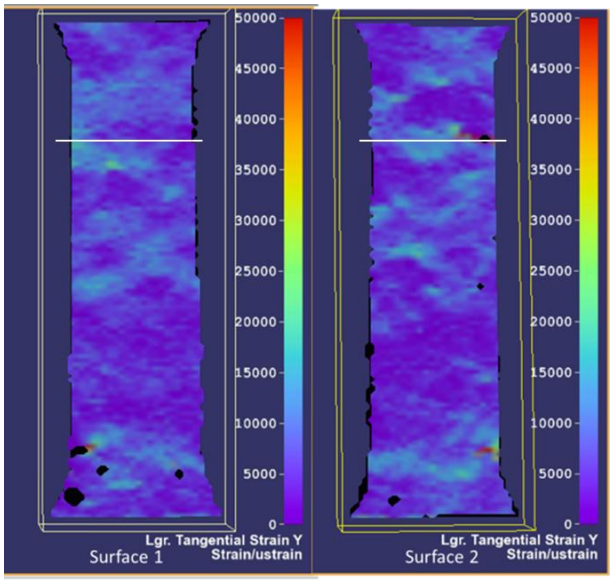

Figure 8: Full field strain plot for 2mm DCFP. Approximate plane of failure indicated by line.

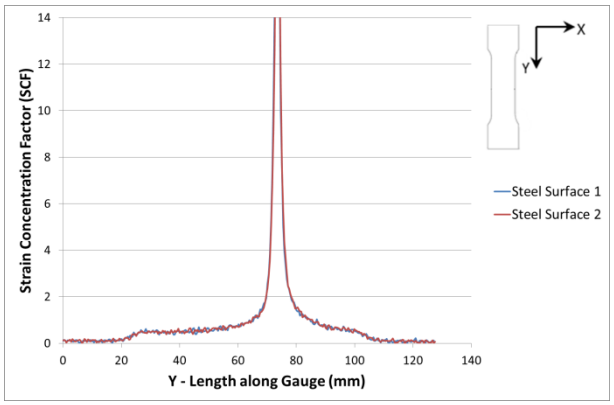

Figure 9: Strains along linear gauges: steel

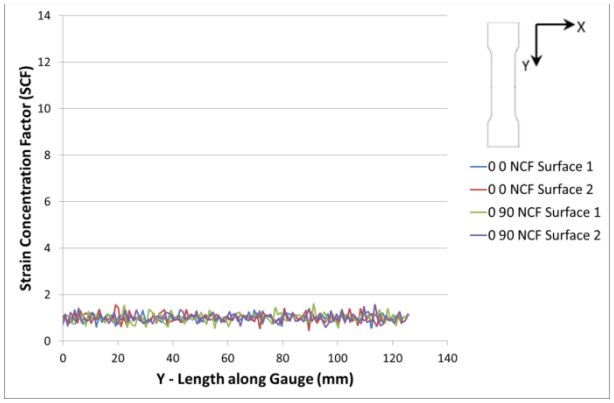

Figure 10: Strains along linear gauges: 0°/90° and 0°/0° NCF

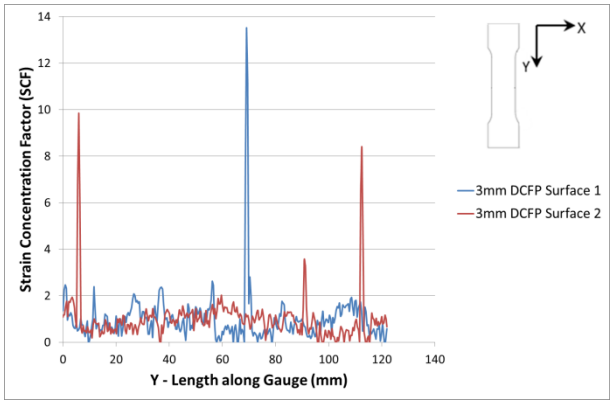

Figure 11: Strains along linear gauges: 3mm DCFP

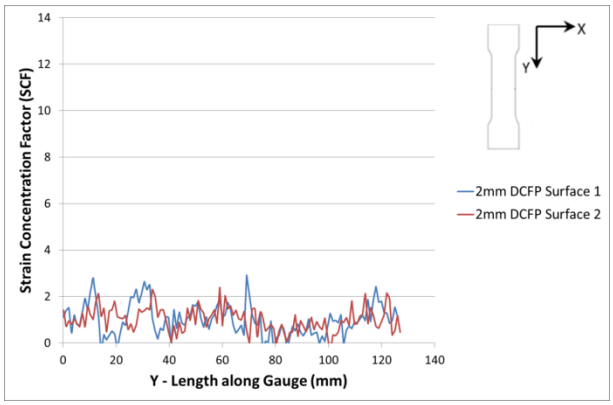

Figure 12: Strains along linear gauges: 2mm DCFP

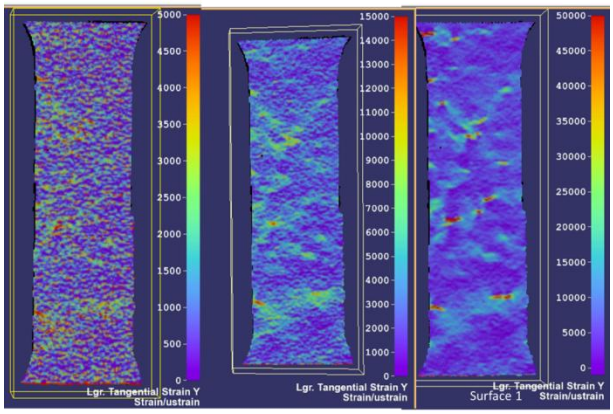

Figure 13: Strain profile for Surface 1 from 3mm thick DCFP sample at applied strain of (Left) 1000 µstrain, (center) 3000 µstrain and (right) 6900 µstrain

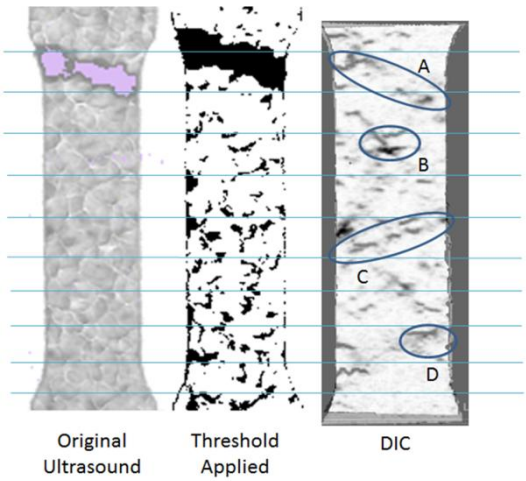

Figure 14: Comparison of DIC and ultrasound. 0-255 grey scale with threshold applied at 110

Table 1: Fiber Volume Fraction (Vf), thickness (t) and summary of tensile properties for each plaque

Plaque	Architecture	Vf (%)	t (mm)	E (GPa)	UTS (MPa)	$\varepsilon_{failure}$ (με)
A	NCF 0/0	40	3	51.0	59.7	11121
B	NCF 0/90	40	3	51.2	65.6	12325
C	DCFP	20	2	9.5	6.7	6209
D	DCFP	40	3	24.8	14.9	6941
E	DCFP	40	6	21.8	16.2	8326

Table 2: Tensile Modulus (GPa) for Steel Sample. Calculated using both rectangular polygon gauges with different facet overlaps (5, 9, 12), different length (large=120mm, small=50mm) and also linear gauges of the same lengths.

Overlap	5		9		12		Linear Gauge	
Gauge Size	Large	Small	Large	Small	Large	Small	Large	Small
Side 1	194.4	192.1	193.5	192.0	194.1	192.1	194.0	190.5
Side 2	193.5	190.3	193.0	189.9	192.3	190.6	192.0	193.1
Average	194.0	191.2	193.3	191.0	193.2	191.4	193.0	191.8
Error between Side 1&2 (%)	0.24	0.48	0.12	0.57	0.47	0.39	0.52	0.68

Table 3: Tensile Modulus (GPa) for Composite Samples

Composite	0°/0° NCF		0°/90° NCF		6mm DCFP		3mm DCFP		2mmDCFP	
Sample	1	2	1	2	1	2	1	2	1	2
Side 1	50.6	51.3	51.8	50.9	21.8	21.1	26.0	23.8	11.1	7.6
Side 2	51.0	51.1	51.8	50.3	22.6	21.5	25.6	23.8	11.5	7.6
Average	50.8	51.2	51.8	50.6	22.2	21.3	25.8	23.8	11.3	7.6
Error between Side 1&2 (%)	0.39	0.20	0.0	0.59	1.80	0.94	0.78	0.0	1.77	0.0